Neutral Particle Spectrometer (NPS) Facility in Hall C

Update to Jefferson Lab PAC 42

May 31, 2014

A. Camsonne, R. Ent, P. Nadel-Turoński, S.A. Wood, B. Wojtsekhowski, C. Zorn
Jefferson Lab, Newport News, VA 23606

A. Asaturyan, A. Mkrtchyan, H. Mkrtchyan, V. Tadevosyan,
S. Zhamkochyan
A.I. Alikhanyan National Science Laboratory, Yerevan 0036, Armenia

M. Guidal, C. Munoz Camacho, R. Paremuzyan
Institut de Physique Nucleaire d'Orsay, IN2P3, BP 1, 91406 Orsay, France

I. Albayrak, M. Carmignotto, N. Hlavin, T. Horn[1]
F. Klein, B. Nepal, I. Sapkota
The Catholic University of America, Washington, DC 20064

C. Hyde, M.N.H. Rashad
Old Dominion University, Norfolk, Virginia

P. King, J. Roche
Ohio University, Athens, OH 45701

D. Day, D. Keller, O. Rondon
University of Virginia, Charlottesville, VA, USA

D.J. Hamilton, J.R.M. Annand
University of Glasgow, Glasgow, Scotland, UK

S. Sirca
University of Ljubljana, Ljubljana, Slovenia

D. Dutta
Mississippi State University

[1] Contact person: hornt@jlab.org

Contents

I. INTRODUCTION

The Neutral Particle Spectrometer (NPS) is envisioned as a facility utilizing the well-understood HMS and the infrastructure of the SHMS to allow for precision (coincidence) cross section measurements of neutral particles. It can be canelevered off the SHMS carriage covering detection angles between 5.5 and 30 degrees, and be positioned on top of the SHMS carriage to cover angles between 25 and 60 degrees. The NPS will be used as photon detector for an approved Deeply-Virtual Compton Scattering [1] experiment, E12-13-010, that aims to extract the real part of the Compton form factors without assumptions. It will also be used as neutral-pion detector for π° electroproduction in semi-inclusive Deep-Inelastic Scattering, in approved experiment E12-13-007, to validate our basic understanding of the partonic interpretation of these reactions with several experimental advantages as compared to likewise charged-pion reactions [2]. Here, the neutral pion will be detected by measurement of its $\gamma\gamma$ decay products.

The NPS could further be used as photon detector for Wide-Angle Compton Scattering [3, 4] reactions, and as neutral-pion detector for exclusive π° photoproduction [5], proposals submitted to this PAC.

The basic concept for the NPS is a highly segmented electromagnetic calorimeter preceded by a compact sweeping magnet. The experiments it enables require detection of neutral particles with energies ranging between ≈ 1 and ≈ 8 GeV, with good energy resolution (1-2%), and good coordinate (2-3 mm) and angular (0.5-1 mr) resolution, comparable to the resolutions of the focusing spectrometers in Hall C. The neutral particle scattering angles cover 6.7-25 degrees for the approved program, and up to 60 degress for the foreseen program. The distance of the calorimeter from the target ranges from 3 to 12 meters. As an example, the minimum angle of the approved program at a distance of 4 m is 7.2°.

The NPS is an efficient and economical way to meet all of the presently known experimental requirements. It will consist of the following components:

- $PbWO_4$ crystals in a temperature controlled frame;
- a set of high voltage distribution bases with built-in amplifiers [6] for operation in high-rate environments;
- essentially deadtime-less digitizing electronics to independently record the pulse amplitudes from each crystal;
- a sweeping magnet of roughly 0.3-0.6 Tm;
- a cantelevered platform of the SHMS carriage to allow precise, remote rotation around the Hall C pivot over an angular range between 5.5 and 30 degrees;
- a platform to mount the NPS on top of the SHMS carriage to allow precise, remote rotation around the Hall C pivot over an angular range between 25 and 60 degrees;
- a light monitoring and curing system to monitor and restore crystal optical properties.

A more detailed description of the NPS facility is in a document submitted to PAC40 [7]. In this update document we will highlight present planning, and progress and results from some of our studies on the critical components of the calorimeter, leading towards a small prototype. We will present some of the results from our studies on LEDs used for gain monitoring and possible curing, phototube sensitivity to infrared light, plans for crystal irradiation and curing tests, as well as details and progress of assembly of the prototype and its LED curing system.

II. NPS CALORIMETER

The NPS calorimeter will consist of an array of up to 1116 scintillating $PbWO_4$ and up to 208 PbF_2 crystals, covering a solid angle of 25 msr at a distance of 4 m from the target. In general, the NPS requires

crystals with high transparency, high light yield, good timing where 90% of the light is emitted within 30-50 ns, and good radiation hardness. Also important are crystal geometry and integrity.

In the ideal case, the NPS calorimeter will consist of a set of brand new $PbWO_4$ crystals. Taking advantage of the existing $PbWO_4$ crystals (and accompanying photomultiplier tubes (PMTs)) of the high-resolution inner part of the Hybrid Electromagnetic Calorimeter (HYCAL) [8] used for the PrimEx/PrimEx-II experiments, one arrangement is an assembly of 1080 $PbWO_4$ crystals in a 36 by 30 matrix. Our goal is to acquire new $PbWO_4$ crystals, both to allow flexibility of scheduling of experiments at Jefferson Lab (given that more and more experiments plan to use $PbWO_4$ crystals) and to increase radiation hardness. Nonetheless, given the worrying lack of qualified vendors of $PbWO_4$ crystals in the world, and to evade scheduling conflicts, we investigate an alternate arrangement consisting of $\approx$ 600 $PbWO_4$ crystals and the available 208 PbF_2 crystals from the Hall A DVCS calorimeter, to complete a calorimeter with similar solid angle. The 600 $PbWO_4$ and $\approx$200 PbF_2 crystals would provide a hybrid calorimeter configuration. A similar but not identical hybrid calorimeter was succesfully used in the PrimEx HYCAL calorimeter, which had an inner core of $PbWO_4$ and an outer ring of lead glass crystals.

A. Choice of Crystals

Analysis of general properties of heavy crystals used in calorimetry show that BGO, $PbWO_4$, PbF_2 and LSO/LYSO are among the candidates. BGO is a commonly used scintillation crystal with a timing property of 300 ns, and is not suitable for the NPS calorimeter. LSO/LYSO crystals have acceptable timing properties, but do not provide an economically favorable option as they would be prohibitively expensive for our envisioned sizes.

Both $PbWO_4$ and PbF_2 crystals are fast, 5-14 ns for $PbWO_4$ and $<$30 ns for PbF_2, and are suitable for experiments requiring fast signals with short tails to minimize pile-up at high rates. This choice is of course also dictated by availability of these type of crystals used in JLab DVCS and PrimEx experiments.

Since the NPS calorimeter may by necessity perhaps be a combination of $\sim$600 $PbWO_4$ blocks (from PrimEx) and 208 PbF_2 blocks (from Hall A DVCS), the component studies should be optimized to include this possibility. This includes taking into account that for $PbWO_4$ crystals the mechanism of light emission is pre-dominantly scintillation, while it is pure Cherenkov radiation for PbF_2. The difference in dimensions and optical properties of $PbWO_4$ and PbF_2 crystals may similarly require different intensity for light monitoring.

B. Crystal Transmittance Measurements

One obvious question that needs addressing for a hybrid calorimeter is if we could use a single primary light source for both $PbWO_4$ and PbF_2 crystals. Hence, we first have to know the transmittance of light for both types of crystals.

We measured the transmittance of $PbWO_4$ and PbF_2 crystals using an existing setup of Jefferson Lab's Radiation Detector and Imaging group, in the ARC. The results are shown in Fig. 1. Comparison of the transmittance curves illustrates that $PbWO_4$ and PbF_2 crystals are very similar in the region above λ $\sim$400 nm, even if different in the short wavelength region (λ $\sim$250-350 nm). Hence, for instance blue light with a wavelength $\sim$470 nm should be acceptable for both types of crystals as a common light source for a monitoring system.

Note that the output pulse timing and shape for the crystals will be different. It would be preferable to use the same digital filtering for actual physics events and light pulser events, but if this difference is significant it may require a different digital filtering.

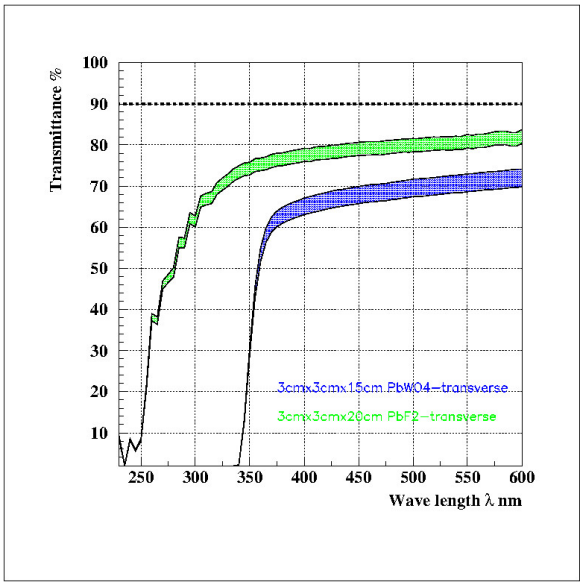

FIG. 1: *Light Transmission efficiencies of the PbF_2 (green) and $PbWO_4$ (blue) crystals (3.0 cm thickness) versus light wave length. Color bands represent spread in data measured at different points of the crystals.*

III. CURING SYSTEM AND COMPONENT STUDIES

All known crystals suffer from radiation damage. The most common damage phenomenon is radiation-induced absorption (reduction in crystals light attenuation length). Previous studies show that the $PbWO_4$ crystal scintillation mechanism is not damaged up to a radiation dose of 2.2 Mrad. Radiation damage of the crystals themselves show a clear saturation, and both transmittance and light yield are stabilized after an initial dosage of a few tens to 50-100 krad, with the level of damage at saturation being dose dependent. Naturally, the radiation damage will depend on the chemical composition of the crystals, and the type and amount of the dope material.

Studies of the radiation conditions in Hall C show that during the planned experiments the accumulated radiation dose may well exceed 100-200 krad, especially for small-angle operation of NPS. To keep the calorimeter performance at the required precision level of understanding efficiency and resolution, we plan to develop a light curing system, and periodically use this between different kinematic settings of the experiments, or whenever the accumulated dose will reach ∼50 krad.

A. General Concepts of Curing System

To restore the crystal optical properties, a curing system will be developed with as minimum impact on the running of the experiments. Our baseline method is to use blue light of wave length between 400 and 500 nm for so-called optical bleaching. It is well established that blue light is most effective in removing the radiation damage and resetting the crystal's attenuation length. The required light intensity is of an order of 1-2 mW/cm^2, and thus for the NPS 20×20 mm^2 ($PbWO_4$) or 30×30 mm^2 (PbF_2) crystals we need a curing system with power of 5-10 mW/crystal. Standard curing with blue light can be very effective: nearly 90% of the original signal can be restored within first 200 minutes with a photon flux of $\sim 10^{16}$ γ/s. However, the technique is invasive (requiring turning PMTs off and Hall access), and based on experience with the Hall A/DVCS experiment can affect PMT operation.

Thus, we also plan to study a curing system with permanent infrared illumination based on those from, *e.g.*, Refs. [9, 10]. Studies show that at such longer wavelengths (600-1000 nm) a significant recovery is possible,

but for a long time of irradiation. This is proven to work very well for low doses (∼3 krad) and can be operated remotely without access to the experimental area. The main difficulty of this method is the lower efficiency, by a factor of 20-50 relative to blue light, which then must be compensated by an increase of the light intensity (up to $\sim 10^{16}$ photons/s per block).

We plan to design, build and test both systems, based on blue and on permanently installed super bright infrared light ($\lambda \geq$940 nm). To be compatible with the NPS, they will have similar mechanical design. For both the curing and the light monitoring systems, detailed studies and selection of the most effective Light Emitting Diodes is critical.

B. Selection of Blue and Infrared LEDs

It is important to select LEDs that can withstand ∼1 Mrad or higher radiation doses without significant degradation (radiation hard LEDs). This strongly depends on the material used in LED production. The best radiation hardness are shown by LEDs based on SiC, GaN and AlGaInP (see [12, 13] and references there). Radiation hardness of the LEDs has been tested with protons, neutrons and photons. It was shown that for GaAs-based LEDs the normalized light output drops by factor ∼5 after radiation doses of 5×10^8 - 10^{10} p/cm^2 caused by protons or neutrons, the degradation effect from photons is 100-1000 times lower: for an accumulated dose of ∼1 kGy (∼100 krad) from photons no noticeable change in the light output or timing characteristics of GaAs-based LEDs was observed.

1. Infrared LED Studies

We have used a test setup of the Radiation Detector and Imaging Group to measure the absolute intensity of several types of blue (RL5-5515, RL5-4630 and SLA-580BCT3F) and infrared (NIR LD-274-3 and TSAL7400) LEDs. Some details of the setup are shown in Fig. 2. The infrared LED (seen on the left) is mounted on a special support structure. The calibrated Photodiode S2281 (seen on right) with an effective area of 100 mm^2 and quantum efficiency of ∼ 67% (at λ ∼950 nm) measures intensity of the emitted light (its current is nearly linearly proportional to the LED intensity). The distance between LED and Photodiode can be varied from 0.5 cm to 20 cm. The LED driving current is measured by a FLUKE multimeter and the Photodiode current is measured by high accuracy KEITHLEY picoamperemeter.

All equipment is installed in a *mini-dark-room*. With closed doors the photodiode dark current, with LED OFF was on the level of ∼0.001 nA. With the doors open the dark current value jumped to 1.1 μA (about 1000 times higher). Though all the LED studies were done with closed doors, this value of dark current is so small that one could do measurements with the doors open.

The electronic circuit which drives the LED used a fixed 5.0 V of the power supply. The value of the LED driving current was then changed over the range from 0 to 100 mA by changing the value of a 1 kΩ variable resistor. We then measured the LED emission intensity versus this driving current with the photodiode located at distances of both ∼3 cm and ∼7 cm from the LED. Results for both infrared LEDs are shown in Fig. 3. At a distance of ∼3 cm, where the LD-274-3 LED fully illuminates the calibrated photodiode (with an effective area of 100.0 mm^2) the energy output is equivalent to 2×10^{16} $\gamma/sec/cm^2$.

The wavelength of the LD-274-3 LED is λ=950 nm at the peak intensity. Using this number as an average to estimate energy of the photons, one obtains an equivalent energy of 1.3 eV:

$$E_\gamma = h \times \nu = h \times c/\lambda = (6.63^{-34}\ m^2kg/s \times 3 \times 10^8\ m/s)/(950 \times 10^{-9}\ m) \approx 1.31\ eV. \quad (1)$$

A photon flux $N_\gamma = 2 \times 10^{16}\gamma/s$ will then deposit a power of $P_\gamma = N_\gamma \times E_\gamma = 2 \times 10^{16} \times 1.31\ eV/s \approx 4.2\ mW$ per cm^2 (at a mean wavelength of 950 nm and at a nominal maximum current of 100 mA driving the LED, as listed in the Osram data sheet).

The data show that the emission intensity is almost linear with driving current. Beyond 60 mA, the output begins to curve slightly indicating the onset of saturation of the emission intensity of the LED. We verified that

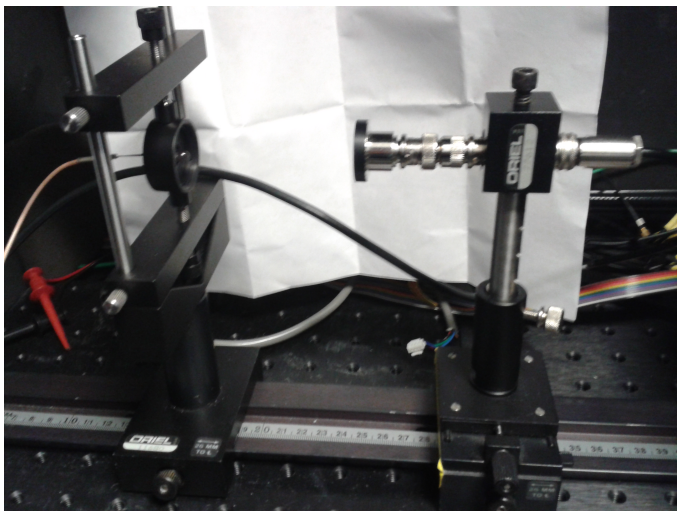

FIG. 2: *LED test setup. An infrared LED (on the left) is mounted on a special support structure. The calibrated Photodiode S2281 (on the right) with an effective area of 100 mm^2 measures the intensity of the emitted light. The distance between LED and Photodiode can be varied from 0.5 cm to 20 cm.*

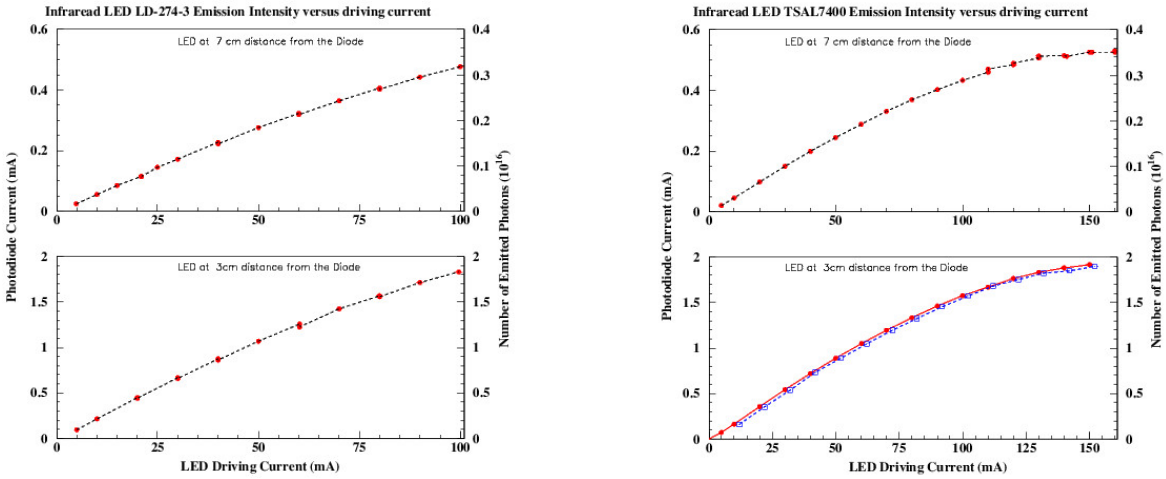

FIG. 3: *Emission intensity of the Infrared LED LD-274-3 (left) and TSAL7400 (right) versus driving current at distance 7 cm (top) and 3 cm (bottom).*

this saturation is due to the LED and not the photodiode by doing additional measurements with attenuation of the LED light output, by installing neutral density filter with attenuation factor of 9.25 in front of the LED. The data without filter and with filter, when scaled by the attenuation factor, are in good agreement.

2. Blue LED studies

The same experimental setup and the same technique were also used to study the emission intensity of several types of blue LEDs, as a function of both the driving current and the distance from the photodiode. Data for a distance of ∼3 cm are shown in Figs. 4 and 5.

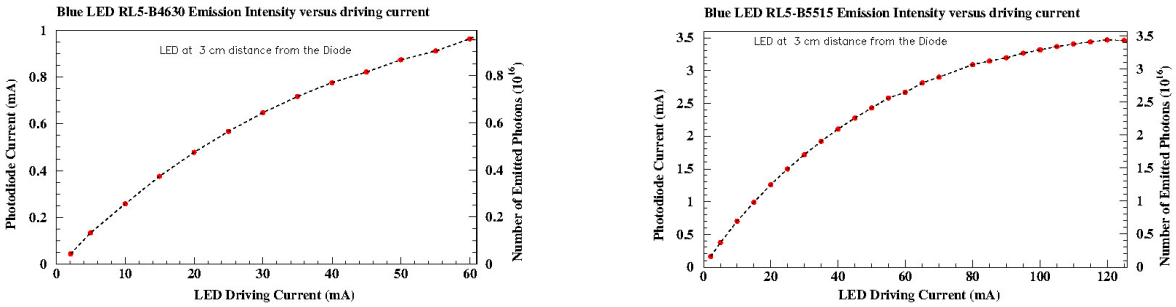

FIG. 4: *Emission intensity of the Blue LED RL5-B4630 (left) and RL5-B5515 (right) versus driving current at a distance of 3 cm.*

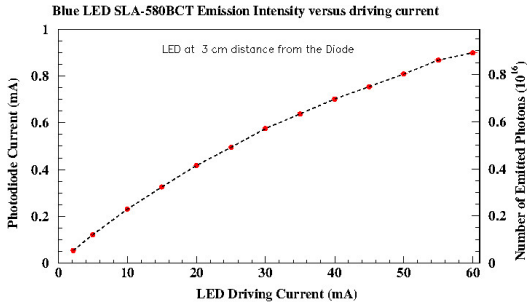

FIG. 5: *Emission intensity of the Blue LED SLA-580BCT versus driving current at a distance of 3 cm.*

C. R4125 phototube sensitivity to Infrared light

The main limiting factor for the IR LED based curing system for the NPS can be the small yet remaining PMT sensitivity to infrared light. It is assumed that IR LED curing would be conducted continuously during the experiment without interruption of data taking with the PMT high voltage ON. For such a requirement it is crucial to know:

- at what level the continuous use of an IR LED will change the PMT anode current, and
- if this rise of anode current will have a negative impackt on the PMT linearity, gain, and lifetime.

For all types of PMTs operating in a high background condition (with high rate and/or high anode current) the limiting factors are the lifetime of the photocathode and the gain. Photocathode lifetime is defined by the amount of charge passing between the photocathode and the first dynode after which the PMT quantum efficiency drops by factor ∼2 from its nominal value. The PMT gain-lifetime is defined by amount of total charge passing through anode which results degradation of the PMT gain by a factor of two.

CMS studies show that after some amount of charge collection the PMT characteristics, apart from the gain, do not show any significant change from their values at the start of the measurement: in Ref. [15] the results of a complete test of 2000 Hamamatsu R7525HA phototubes for the CMS forward hadron calorimeter are reported. This is an 8-stage PMT with 25 mm diameter of Bialkali photocathode, with gain $\sim 5 \times 10^5$ at high voltage 1750 V, and typical anode dark current of 5 nA (maximum ∼100 nA). The studies found that the relative drop in the gain after 3000 C of charge collection depends on the High Voltage (or gain) and may vary from ∼2 (at low HV) to 5 (at high HV).

In general, pending on the type of PMT, the photocathode and dynode materials, the mechanical construction and the operation regime, the photocathode-lifetime may well vary from a few tens to a few hundred mC, while the gain-lifetime may vary from few hundred to few thousand C. As a consequence, to prolong the PMT lifetime one needs to keep the cathode and anode currents as low as possible. This is also required for

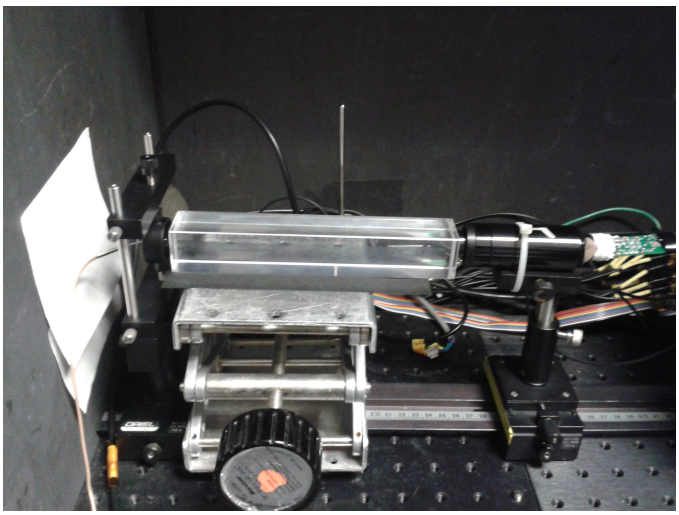

FIG. 6: *Experimental setup for the PMTs sensitivity measurements to infrared light. A 20 cm PbF_2 crystal is installed between the PMT and the LED.*

as minimum as possible dark currents of the PMT. Any additional source which may increase the PMT anode current (dark current) will have a negative impact on the lifetime of the PMT. Thus, curing of the crystals in situ by using a high-intensity infrared light without turning the phototube high voltages off is in practice only possible if the rise of the PMT dark current when the infrared LED is on is completely negligible relative to the anode current, or less than a few times of the nominal dark current.

The possibility to perform continuous curing of the crystal in-situ (with the PMTs' HV on) using infrared light with wavelength $\lambda \geq$900 nm depends thus on the (quantitatively unknown) quantum efficiency of the PMT in this wavelength region. Since effective curing will require a very high IR light intensity ($\geq 10^{17}$ γ/sec) this is even an issue for a small quantum efficiency this IR wave lenght: the phototube could still be completely damaged with such a high intensity IR light.

We thus measured the R4125 phototube's sensitivity to the infrared light. The tube was installed on front of the LED. The measurements were done at different driving currents of the LED (from 0 up to 100 mA), at distances of 0.5 cm and 16 cm (18 cm), with and without a PbF_2 ($PbWO_4$) crystal placed in front of the PMT, and at different gains of the PMT. For these measurements we used one of the prototypes of the active divider with built-in amplifier we developed earlier for this PMT, to increase linearity up to high rates. In the measurements, we first measured single electron peak and gain of R4125. At high voltages of 1600, 1700 and 1750 V, respectively, we found the following gain values: 3.8×10^7; 7.6×10^7 and 1.0×10^8. These values are much higher than those listed in the Hamamatsu data sheet (gain of 10^5 at 1500 V) due to the use of the active divider.

To measure the PMT quantum efficiency at wavelengths far beyond the sensitivity range specified in the Hamamatsu data sheet, in the infrared, the output signal was sent to an ADC, and we used a simple DAQ system based on Lab-VIEW. The ADC gate width was set to be 150 nsec, and a channel was equivalent to 100 fC. Data for each setting were taken for 5 min (300 sec) with a frequency of $\sim$200-300 Hz. Amplitude distributions of the signals were detected at different driving currents through the IR LED LD-274-3 and TSAL7400 type LEDs. We then repeated the measurements with a crystal (PbF_2 or $PbWO_4$) installed between the LED and the PMT, as shown in Fig. 6.

The data suggest that PMT R4125 has a very low, yet not negligible, quantum efficiency relative to infrared light. As example, we show in Fig. 7 the amplitude distributions of the signals detected by the R4125 PMT at different values of the driving currents of the infrared LED NIR LD-274-3. It is possible that the PMT sensitivity may be due to contamination by short wavelength light of the IR LED spectrum. Tests were thus repeated with a 900 nm filter cutting all wavelengths but IR. No difference between the measurements with and

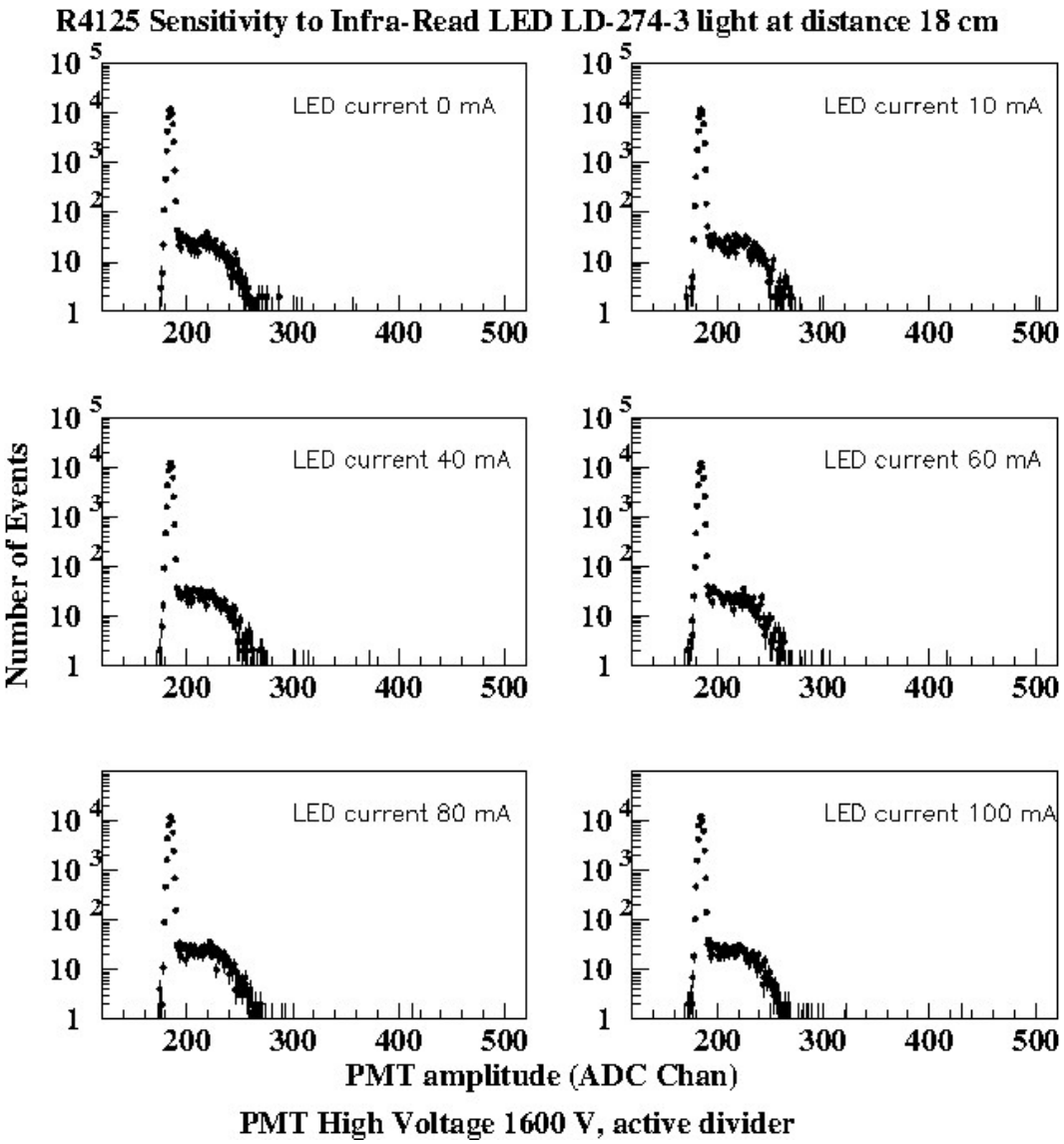

FIG. 7: *The amplitude distributions of the signals detected by PMT R4125 at different values of infrared LED NIR LD-274-3 driving currents.*

without filter were found. This suggests that the majority of the light has IR wave length, that the PMT has a non-zero efficiency with respect to IR light, and that the PMT could thus potentially receive long-term damage if left on during *in situ* IR curing. More studies are ongoing, for instance given the sensitivity to wavelengths $\lambda \geq$900 nm, we may also search for suitable LEDs with an emission spectrum >1000 nm.

To start studying potential damage of the PMT during long-term operation, we measured the PMT R4125 anode current versus driving current of IR LEDs LD-274-3 with the PMT at high voltage settings of 1400 V, 1500 V and 1600 V, respectively, when a single IR LED or a matrix of four IR LEDs illuminated the photocathode. Some results of the measured anode currents with the PMT set at a high voltage of 1600 V are shown in Fig. 8.

With the high voltage of the PMTs on, and no LED driving current, the dark current of the PMT is 11 nA for 1400 V, 18 nA for 1500 V and 28 nA for 1600 V, respectively. Then, for the case where a single LED is positioned at a distance of 19 cm of the front of the PMT, and an LED driving current of 50 mA, the anode current is 309 nA for 1400 V, 492 nA for 1500 V and 758 nA for 1600 V, respectively. For reference, for a similar 50 mA driving current and a matrix of four IR LEDs at this distance, the photon flux would be $\sim 10^{17}\ \gamma/cm^2$/sec. This corresponds to a total charge passing through the PMT due to dark currents of only

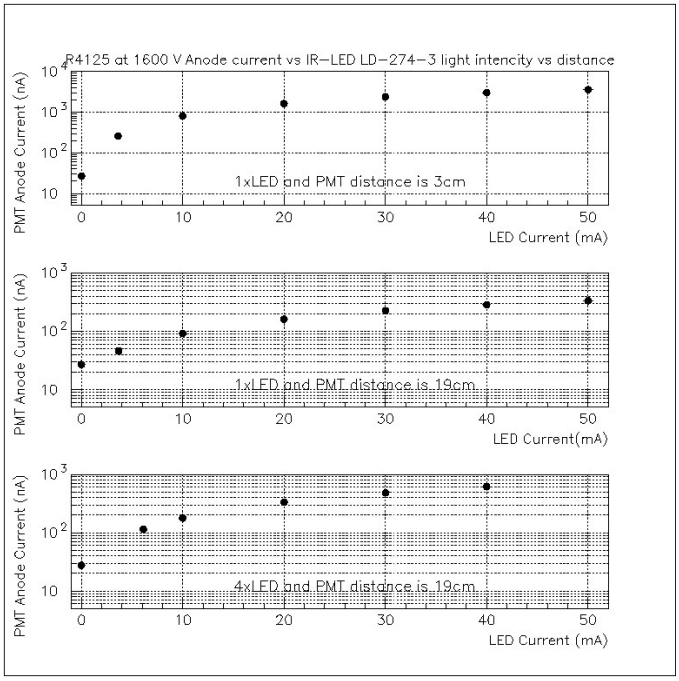

FIG. 8: *PMT anode current, at a high voltage setting of 1600 V, versus the driving current of IR LEDs: (top)- use of one LED positioned at distance 3 cm from the PMT; (middle)- similar, at a distance of 19 cm from the PMT; and (bottom- a matrix of four LEDs at a distance of 19 cm from the PMT*

.

∼3C, for a 1000 hour run (at a high voltage of 1600 V).

The maximum anode current for the R4125 PMT is ∼0.1 mA. The gain of the PMT, using the active divider (with amplifier), is $\sim 3.8 \times 10^7$ at a high-voltage setting of 1600 V. Most likely we will only require a gain in the 10^5 gain range, and not use high voltage settings higher than 1400-1500 V. Thus, there may not be an adverse effect on the PMT, yet it is clear that more study is needed. For the distance of 19 cm, close to the anticipated geometry using ∼18 cm $PbWO_4$ crystals or ∼20 cm PbF_2 crystals sandwiched between the PMT and LED, the PMT dark current values are listed versus the LED driving current in Table 1.

I_{LED} (mA)	I_{Anode} (nA)	I_{LED} (mA)	I_{Anode} (nA)
0.0	27	0.0	27
3.7	46	6.0	114
10.0	92	10.0	177
20.0	161	20.0	334
30.0	225	30.0	478
40.0	284	40.0	609
50.0	332	53.0	758

TABLE I: R4125 phototube anode dark current at an operating high voltage of 1600 V versus the LD-274-3 driving current. The left half of the table illustrates the case when using a single LED, the right half for the case of using a matrix of four LEDs. In each case the PMT was located at a distance of 19 cm from the LED(s).

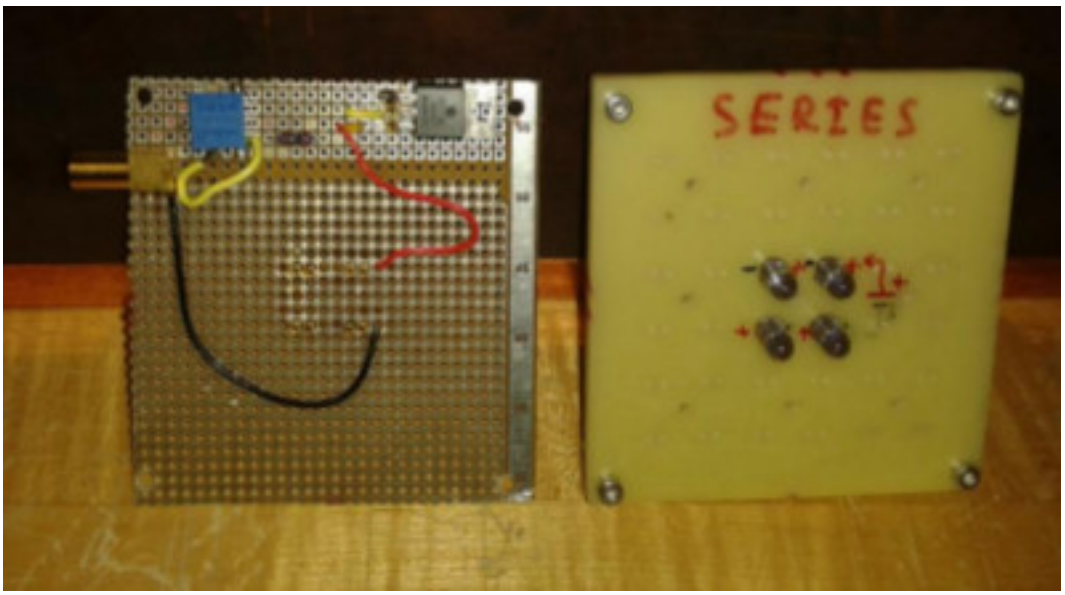

FIG. 9: *Partly assembled Infrared LED curing system.*

IV. FURTHER STUDIES AND PROTOTYPING

A. Design and construction of the curing system

For further tests we plan to make two versions of the curing system. In the first version, the curing will be performed with a matrix of 4 ultra-bright Blue LEDs per block (with intensity about 10^{16} γ/sec per block). The second version would be a clone of the first one, but with a matrix of 4 ultra-bright Infra-Red LEDs per block (with intensity about 5×10^{17} γ/sec per block). In each case, the matrix of ultra-bright LEDs will be mounted at small distance from the crystals. In Fig. 9 we shown a partly assembled prototype curing system.

B. Irradiation of the $PbWO_4$ crystals

We further plan to do controlled irradiation and curing studies of the various crystals. To this end, we plan to use four $PbWO_4$ crystals, each with dimensions $\sim 1.5 \times 1.5 \times 2.0$ cm^3 for radiation tests. Three of these crystals are passed on to the Jefferson Lab Radiation Control group who have a small facility that can provide controlled doses with a ^{137}Cs gamma source. We plan to irradiate with up to $\sim$20 krad dose each step. The fourth crystal will serve as a reference in the measurements. One of the radiated crystals will be used for tracing spontaneous recovery with time, the two others will be used for curing studies with blue and infrared lights. We plan to monitor the curing effect by intermittent light transmission measurements of the crystals. This work has just started.

C. Prototype Design

Taking into account the possibility of construction of the NPS calorimeter as a combination of $PbWO_4$ and PbF_2 crystals, we have designed a prototype frame that could include both scenarios: a matrix of 3 by 3 $PbWO_4$ crystals, and a matrix for the $PbWO_4/PbF_2$ hybrid case (3 by 2 $PbWO_4$ crystals and 2 PbF_2 crystals. We plan to again use the 19 mm diameter R4125 Hamamatsu PMTs as used in the PrimEx hybrid calorimeter, with our active dividers. We have acquired 10 $PbWO_4$ crystals from SICCAS for our prototype, with quality close to the $PbWO_4$ crystals used by CMS.

D. The Light Monitoring system

A light monitoring system will measure variations of the transmittance of crystals in the course of experiment and provide calibration *in situ*. It will be used to control stability of the detector, degradation of the crystals due to accumulated radiation and define condition when curing of the crystals is needed. It will periodically inject light into the detector modules between the real events during data taking, or during special calibration runs with a frequency 10-20 Hz.

There are three important factors which must be taken into account when considering a light source for the system. First, the source should be as stable as possible. The reference photodiode coupled to it will take out pulse-to-pulse instabilities, but it is still useful to have the primary light source stable in short and long time scale. The second factor is light intensity. Intensity of the light delivered to the large number of crystals in the calorimeter must have an equivalent energy of around 1-3 GeV in each of the crystals. The third factor is timing distribution of the pulses. It must be similar to that from the real event (scintillation pulse for $PbWO_4$ and Cherenkov pulse for PbF_2).

We are studying an LED-based monitoring system to control the status of the $PbWO_4$ blocks and the PMT gains in the course of experiments. The light source is an assembly of NICHINA Super Bright NSPB500AS LEDs located outside of the prototype in radiation safe area. Light from this LED assembly will mix and be delivered to the prototype by ~ 200 μm fiber. There is a special ST type optical fiber connecter on the prototype frame for to plug this primary fiber.

Inside of the prototype box this light will split and delivered to each crystal by bandle of fibers: one monitoring fiber per block. One end of all fibers will be bound together and fed into the ST connector, the second end of the fibers will plug into a hole of an envisioned led-holder plate.

[1] E12-13-010, Exclusive Deeply-Virtual Compton and Neutral Pion Cross Section Measurements in Hall C, Approved by Jefferson Lab PAC40, C. Munoz-Camacho, R. Paremuzyan, T. Horn, J. Roche, and C. Hyde, spokespersons.
[2] E12-13-007, Measurement of the Semi-Inclusive π° Production as Validation of Factorization, Approved by Jefferson Lab PAC40, T. Horn, R. Ent, H. Mkrtchyan, V. Tadevosyan, spokespersons.
[3] Wide-Angle Compton Scattering at 8 and 10 GeV Photon Energies, Deferred proposal by PAC40, updated proposal submitted to PAC42, D.J. Hamilton, S. Sirca and B. Wojtsekhowski, spokespersons.
[4] Initial State Helicity Correlation in Wide Angle Compton Scattering, Proposal submitted to PAC42, D. Day, D. Keller and J. Zhang, spokespersons.
[5] Large Center-of-Mass Angle, Exclusive Photoproduction of π° Mesons at Photon Energies of 5-11 GeV, LOI12-13-003 submitted to PAC40, proposal submitted to PAC42, D. Dutta, H. Gao, M. Amaryan, S. Sirca, I. Strakovsky, spokespersons.
[6] V. Popov, H. Mkrtchyan, New potomultiplier active base for Hall C Jefferson Lab Lead Tungstate Calorimeter, NSSS2012-1098.
[7] Neutral Particle Spectrometer Facility in Hall C, NPS collaboration, https://hallcweb.jlab.org/experiments/PAC40/
[8] M. Kubantsev et al., Performance of the Primex Electromagnetic Calorimeter, arXiv:physics/0609201, 22 Sept. 2006; A. Gasparian, Proceed. X Int. Conf. Calorimetry in Part. Phys., Perugie, Italy, 29 March-2 April 2004, pp. 109-115
[9] M. Anfreville et al., Nucl. Instrum. Meth. A**594**, 292 (2008).
[10] R.W. Nowotny, PANDA Collaboration, IEEE-2009-05402124.
[11] R. Zhu, L. Zhang, Quality of Mass-Produced Lead Tungstat Crystals, IEEE Transact. on Nucl. Science, 51 (2004) 1777-1783
[12] Characterization of Proton Damage in Light-Emitting Diodes, A. H. Johnston and T. F. Miyahira, IEEE Trans. Nuclear Science 47 (2000) 2500-2507
[13] Energy Dependence of Proton Damage in AlGaAs Light-Emitting Diodes, R. A. Reed et al., IEEE Trans. Nuclear Science 47 (2000) 2492-2499
[14] A Precision Measurement of the Neutral Pion Lifetime via the Primakoff Effect, PrimEx Conceptual Design Report, Primex Collaboration, Jefferson Lab, March 3, 2000
[15] Complete Tests of 2000 Hamamatsu R7525HA phototubes for the CMS-HF Forward Calorimeter, U. Akgun et al. Nucl. Instr. Methods, A 550 (2005) 145-156